Bioactive Materials 10 (2022) 107–116

Contents lists available at ScienceDirect

Bioactive Materials

journal homepage: www.sciencedirect.com/journal/bioactive-materials

Seamless integration of bioelectronic interface in an animal model via *in vivo* polymerization of conjugated oligomers

Giuseppina Tommasini [a,1], Gwennaël Dufil [b,1], Federica Fardella [a], Xenofon Strakosas [b], Eugenio Fergola [a], Tobias Abrahamsson [b], David Bliman [c], Roger Olsson [c,d], Magnus Berggren [b], Angela Tino [a], Eleni Stavrinidou [b,**], Claudia Tortiglione [a,*]

[a] *Istituto di Scienze Applicate e Sistemi Intelligenti "E. Caianiello", Consiglio Nazionale delle Ricerche, Via Campi Flegrei 34, 80078, Pozzuoli, Italy*
[b] *Laboratory of Organic Electronics, Department of Science and Technology, Linkoping University, SE-60174, Norrkoping, Sweden*
[c] *Department of Chemistry and Molecular Biology, University of Gothenburg, SE-405 30, Gothenburg, Sweden*
[d] *Chemical Biology & Therapeutics, Department of Experimental Medical Science, Lund University, SE-221 84, Lund, Sweden*

ARTICLE INFO

Keywords:
In vivo polymerization
Bioelectronics interfaces
Conjugated oligomers
Model organism

ABSTRACT

Leveraging the biocatalytic machinery of living organisms for fabricating functional bioelectronic interfaces, *in vivo*, defines a new class of micro-biohybrids enabling the seamless integration of technology with living biological systems. Previously, we have demonstrated the *in vivo* polymerization of conjugated oligomers forming conductors within the structures of plants.

Here, we expand this concept by reporting that *Hydra*, an invertebrate animal, polymerizes the conjugated oligomer ETE-S both within cells that expresses peroxidase activity and within the adhesive material that is secreted to promote underwater surface adhesion. The resulting conjugated polymer forms electronically conducting and electrochemically active μm-sized domains, which are inter-connected resulting in percolative conduction pathways extending beyond 100 μm, that are fully integrated within the *Hydra* tissue and the secreted mucus. Furthermore, the introduction and *in vivo* polymerization of ETE-S can be used as a biochemical marker to follow the dynamics of *Hydra* budding (reproduction) and regeneration. This work paves the way for well-defined self-organized electronics in animal tissue to modulate biological functions and *in vivo* biofabrication of hybrid functional materials and devices.

1. Introduction

Bioelectronics aim to monitor, actuate or modulate biological processes. Currently there is a major focus on developing implantable bioelectronic devices expressing a minimal mismatch with the hosting biological environment in order to reduce the foreign body response. Examples include soft [1], conformable electronics [2–4], and ultrathin injectable systems [5]. Recent non-conventional approaches target to integrate directly the electronic material into tissue. Martin and co-workers were the first to exploit this possibility by electropolymerizing PEDOT electrodes directly into the brain of a mouse, which created a cell-templated electrode [6]. However, electropolymerization requires application of high currents via a working electrode that potentially can be harmful for the brain while the formed polymer is only localized in the vicinity of the electrode. In an attempt to induce chemical polymerization, Bao et al. genetically modified neuronal cells to express a biological catalyst, the peroxidase enzyme, on the cell membrane and demonstrated the polymerization of aniline dimers after addition of hydrogen peroxide [7]. Genetic modification is typically imposing several limitations in terms of the applicability of the method. Recently, we presented a thiophene-based conjugated oligomer, ETE-S, that *in vivo* polymerized in a plant without any exogenous physical or chemical stimuli, forming conducting wires along the plant's vascular tissue [8]. The polymerization was driven by the plant's endogenous peroxidase enzymes that are localized in the plant's cell wall therefore naturally integrating the conducting material directly

Peer review under responsibility of KeAi Communications Co., Ltd.
* Corresponding author.
** Corresponding author.,
E-mail addresses: eleni.stavrinidou@liu.se (E. Stavrinidou), claudia.tortiglione@cnr.it (C. Tortiglione).
[1] equal contribution.

https://doi.org/10.1016/j.bioactmat.2021.08.025
Received 24 June 2021; Received in revised form 5 August 2021; Accepted 23 August 2021
Available online 28 August 2021

into the plant structure [9,10]. Leveraging the enzymatic catalytic activity for augmenting non-native functionality into biological systems is indeed a promising route. Living organisms perform a broad range of coordinated catalytic reactions resulting in complex biological functions and biomaterials. Thus, exogenously applied compounds that enter biological reaction networks can result in hybrid systems that combine unique features of living organisms with functionality and performance of artificial materials. We recently exploited this visionary approach also in a small invertebrate animal, *Hydra vulgaris*. The freshwater polyp *Hydra* is typically used as a model system in developmental biology and regeneration studies but since the last decade emerged as a powerful *in vivo* model to test the interaction of a living system with nanostructured materials providing indication on toxicity [11,12], efficiency of cell uptake [13], intracellular fate [14], and biotransformation of exogenous compounds [15]. Taking these studies a step further we recently demonstrated that *Hydra* when treated with a semiconducting oligothiophene, DTTO, is promoting, *in vivo*, the biogenesis of fluorescent conductive protein microfibers via metabolic pathways [16]. Furthermore, in another study, we demonstrated that poly (3-hexylthiophene) P3HT nanoparticles elicit a behavioral response in *Hydra* and induced modulation of genes involved in the light transduction pathways, suggesting a seamless and biomimetic interface between the polymer nanoparticles and the living organism [17].

Along this direction, and also inspired by the possibility of seamlessly integrating electronic devices in animal tissues, endowing themselves with functions beyond the native ones, we exploited the capability of ETE-S conjugate trimer to polymerize into conductive structures within the soft *Hydra* tissue. By simply incubating living polyps in a solution containing ETE-S, the oligomer was uptaken by the animal and spontaneously polymerized at highly localised regions. Optical, spectroscopic and electrical characterization demonstrated that the ETE-S polymerizes in a specific foot cell type that expresses peroxidase activity,

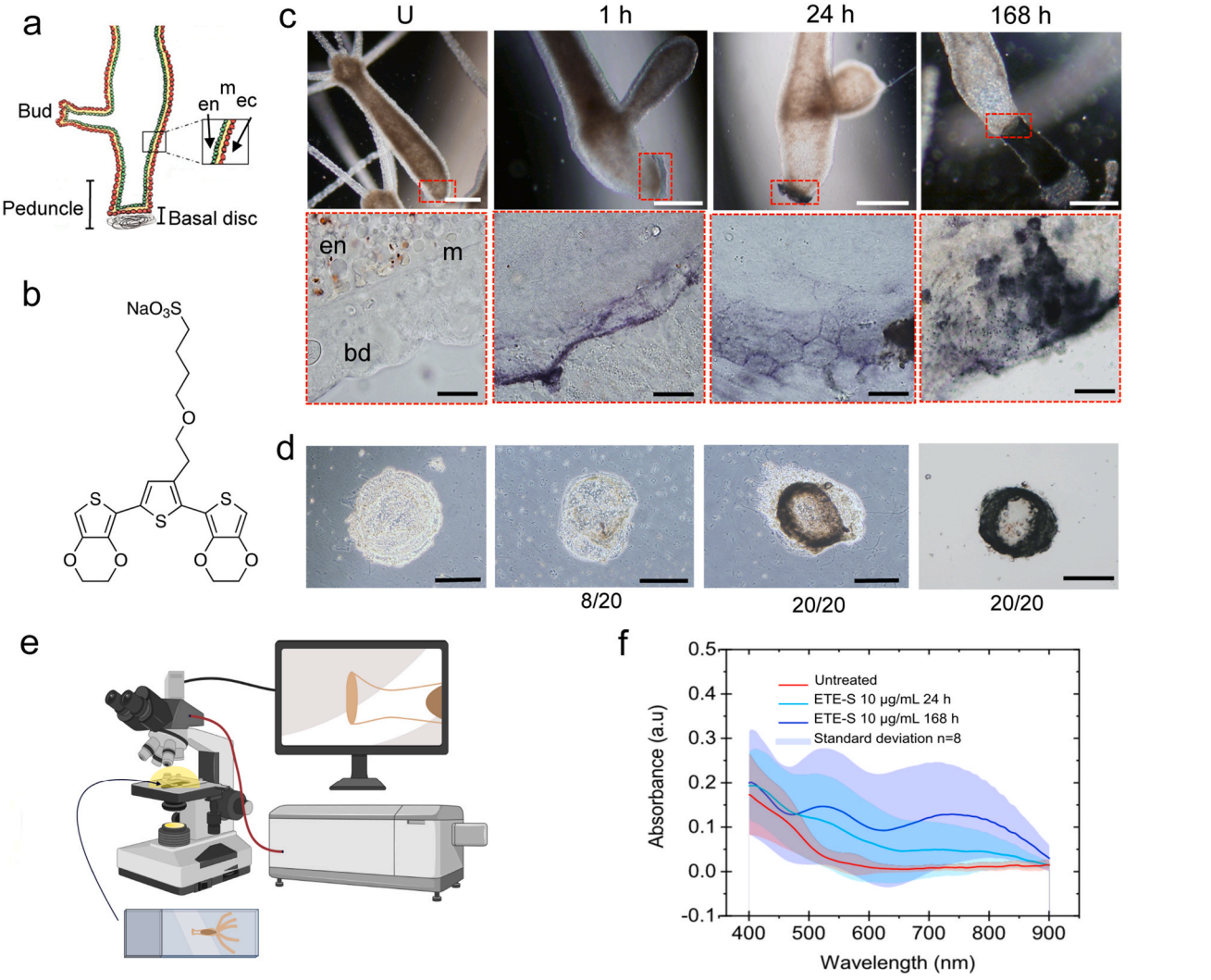

Fig. 1. Temporal dynamics of ETE-S polymerization in *H.vulgaris*.
a) Schematic representation of the lower body region of *Hydra vulgaris*. The tissue is organized into endoderm (en) and ectoderm (ec) cell layers separated by the mesoglea (m). b) Molecular structure of the ETE-S. c) *In vivo* imaging of polyps treated with ETE-S (10 µg/mL). Black stained secreted mucous is detectable since the first hour of incubation, reaching maximal thickness after 1 week. Untreated animals (U column) are shown on the left. In the lower panel images of living polyps squeezed onto a microscope slide reveal the bilayer structure at the base of the peduncle region (red dashed area) including basal disc cells (bd), mesoglea (m) and endoderm. Treated polyps reveal staining of the basal disc cells, initially diffuse (1 h) and then organized into granular structures. Scale bars 500 µm (upper panel), 50 µm lower panel. d) Secreted discs from untreated (left) and treated polyps, whose darkness progressively increases. The number of stained secreted discs on the total of treated animals is indicated at the bottom of each column. Scale bar, 200 µm. e) Schematic of the spectromicroscopy setup where the microscope transmitted light collects the absorption spectra using a spectrophotometer (red cable). The scanned area is targeted live with the help of a camera (black cable). biorender.com. f) Average absorption spectra of dried secreted discs from *Hydra* untreated (red), treated with 10 µg/mL ETE-S for 24 h (light blue) and treated with 10 µg/mL ETE-S for 168 h (dark blue). Standard deviation from n = 8 is shown as the colored halo.

and in the secreted adhesive material used by the polyps to anchor on underwater substrates. The p(ETE-S) functionalized animal tissue and ring-shaped secreted structures acquired electronic conductivity and electrochemical capacitance demonstrating the possibility of augmenting electronic functionality in animals and the biofabrication of electronic hybrids. Our work paves the way on utilizing the innate potential of living organisms to build complex structures and their biocatalytic machinery for transforming chemical stimuli into electrical microdevices.

2. Results and discussion

2.1. In vivo ETE-S polymerization in Hydra vulgaris

Fig. 1a shows a scheme of a longitudinal section of the *Hydra* lower body column, structured into the two cell layers and organised into a peduncle ending with a basal disc, a specialised secretory region responsible for polyp temporary adhesion to underwater surfaces [18]. Despite sessile life, *Hydra* can move by repetitive substrate attachment and detachment, governed by both muscular activity and the secretion of glue, functions which are not completely understood, to date. At the terminal end of the body column, basal disc cells have been identified as responsible for synthesis, storing and delivery of components underlying *Hydra* adhesion [19]. These cells contain different types of granules whose content (glycans, glycoproteins and peroxidase) is in part secreted outside in the external environment [20,21]. We first investigated the potential toxic effect and more broadly the biocompatibility of ETE-S, by monitoring and quantifying morphological alteration induced at variable dose and exposure time, according to well established methods [11,22,23]. Living polyps were incubated with increasing doses of ETE-S, from 10 μg/mL to 1 mg/mL, the effective dose used in plant systems (Fig. S1) [8]. While at 1 mg/mL the animals appeared immediately paralyzed and cell lysis occurred throughout the body, ETE-S at 10 μg/mL had no effect on polyp morphology and behaviour, allowing incubations up to one week without affecting the polyp viability at macroscopic levels. For this reason, 10 μg/mL was further used for long term experiments to detect and monitor *in vivo* polymerization, as recently reported in plants [9,24]. By inspecting the ETE-S treated *Hydra*, a dark staining was detectable at the basal disc level and within the secreted material already after 1 h of treatment (Fig. 1c, upper panel). At higher magnification, in living squeezed polyps (Fig. 1c, lower panel) basal disc cells appeared purple stained, suggesting their involvement in the ETE-S intracellular polymerization. These features progressively increased at longer incubation times leading to the detection of dark granular spots within the cells and embedded into the secreted material outside the polyp (Fig. 1c–d, Fig. S2). The material secreted from basal disc cells, organized as a solid structure (from now named secreted discs), showed the presence of dark material organized as a ring, which thickness increased with the incubation period (Fig. S2), indicative of the continuous ETE-S polymerization and external secretion (Fig. 1d). Secreted discs from untreated *Hydra* incubated with ETE-S do not show any staining (Fig. S2), indicating the absence of the necessary chemical machinery to induce polymerization in the secreted material. In order to confirm the polymerization of ETE-S, we performed spectromicroscopy on isolated secreted discs and on whole *Hydra* polyps (Fig. 1e). For each incubation period, the spectra were collected from 8 different discs and an average spectrum is shown for each time of incubation (Fig. 1f).

In the absorption spectra of secreted discs from *Hydra* treated with 10 μg/mL ETE-S for 24 h a shoulder at the 500 nm region was observed, as well as a broad absorption band at 700–800 nm region. Discs collected at 168 h of continuous incubation showed enhanced absorption signatures, with clearly defined bands at 500 nm and 700–800 nm. The 500 nm band corresponds to the HOMO → LUMO transition for p(ETE-S) and the band at 700–800 nm to p(ETE-S) doped states as previously shown from a combination of spectroelectrochemistry studies and density functional theory (DFT) calculations [8,25]. The doped states can be attributed to either a mix of polaronic and bipolaronic states or only bipolaronic states with pi-stacking effects as suggested by DFT calculations [25]. The fact that the neutral state is present suggests that the formed p(ETE-S) is not fully doped. Both treated and untreated samples had an absorbance band around 400 nm that can be attributed to light scattering from biological tissue.

After observing clear polymerization of ETE-S in the discs of secreted material, we further investigated the possibility of polymerization in *Hydra* tissue, as suggested by the dark-stained tissue observed *in vivo* (Fig. 1c). Spectromicroscopy was performed in polyps treated for 24 h and dried on glass slides. Spectra were acquired from different anatomical regions and compared to untreated *Hydra*. The average absorption spectra show no difference between untreated (Fig. 2a) and ETE-S functionalized *Hydra* (Fig. 2b) at tentacle junction and body levels, suggesting that no polymerization occurred in those areas. Some features were present in both cases suggesting that they arise from light scattering from the tissue. In contrast, spectra from the basal disc region of ETE-S functionalized *Hydra* show the characteristic peaks corresponding to p(ETE-S) as described in the previous section.

Since we were not able to determine p(ETE-S) formation by spectromicroscopy in the whole *Hydra*, we then attempted to solubilize any p(ETE-S) that may be present in the tissue via homogenization in DMSO [8]. Homogenates were prepared from ETE-S treated polyps, whole or sectioned at 20% of total body length in two parts to separate the upper body from the foot region, and then compared to corresponding untreated samples. Fig. 2d shows the characteristic absorbance band at 500 nm in all the functionalized extracts (whole polyp, upper body, and foot) but not in untreated *Hydra* samples, confirming the presence of p(ETE-S). These data are supported from previous studies where we showed that when p(ETE-S) is dissolved in DMSO, it dedopes into the neutral form that displays a characteristic absorption band at 500 nm [8]. Interestingly, these results suggest that ETE-S polymerization occurs not only in the basal disc region, as shown in the spectromicroscopy studies, but also in other regions indicating that the polymerization is not restricted to the foot basal disc cells. This is consistent with the expression of five isoforms of putative peroxidases in the ectoderm, whose functional significance, however, is still unknown [21,26,27]. Most probably the concentration of the p(ETE-S) was highly localized or below the detection limit to be revealed with spectromicroscopy. To verify this hypothesis, we performed *in vitro* reaction using whole fixed polyps (i.e. animals mummified by the use of paraformaldehyde), and high doses of ETE-S (1 mg/mL) and H_2O_2 (0,17%), which would be toxic for live animals. Under this condition a clear polymerization both in the basal disc region and in the upper body part of the *Hydra* was observed, indicating that the upper part tissue can polymerize ETE-S but with relatively lower efficiency (Fig. S3).

2.2. ETE-S polymerization in Hydra is mediated by peroxidase enzyme activity

Starting from spectroscopy analysis detecting ETE-S polymerization in the secreted discs, and from evidence that ETE-S polymerization both in plants and *in vitro* is assisted by peroxidase enzymes [8,9], we investigated this possibility also in *Hydra*, supported by the specific localization of peroxidase activity into the granules of the basal disc cells [19,20,28]. Biochemical and ultrastructural analyses have recently characterized diverse types of secretory granules containing glycans and glycoproteins (found also in secreted material) [19], lipids and peroxidase-like enzymes (Fig. S4), thus the presence of this enzymatic activity is used in reliable assays to identify basal disc cells, in homeostatic conditions or in dynamic processes (i.e. budding and regeneration processes). By adding the substrates of chromogenic reactions catalyzed by peroxidases, such as diaminobenzidine (DAB) and H_2O_2, the oxidation to a brownish product is detectable only in cells with high endogenous peroxidase activity (Fig. S4) [28]. On this basis, we tested the

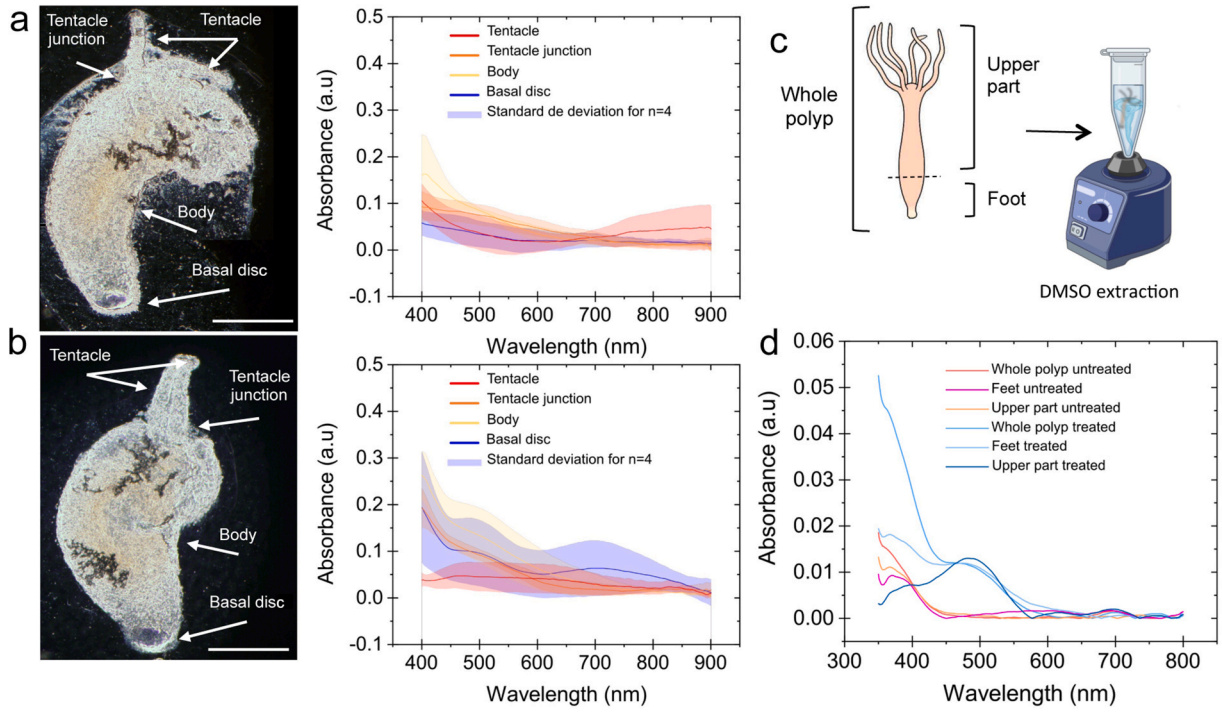

Fig. 2. Optical and spectroscopic characterization of ETE-S treated *Hydra*, in whole and homogenated animals.
a) Micrograph of dried untreated polyp and corresponding average absorption spectra acquired with spectromicroscopy on several anatomical regions: basal disc region (dark blue), body (yellow), tentacle/body junction (orange) and tentacle (red). Standard deviation for n = 4. b) Micrograph of dried polyp treated with 50 μg/mL ETE-S for 24 h and corresponding average absorption spectra. Standard deviation from n = 4 shown as a colored halo. c) Schematic legend of the *Hydra* body parts extracted in DMSO.biorender.com. d) Absorption spectra from DMSO extracts of whole polyps untreated (red) and treated (blue), feet from untreated (rose) and treated (light blue) *Hydras* and upper part from untreated (orange) and treated (dark blue) *Hydras*. Scale bar 500 μm in a, b.

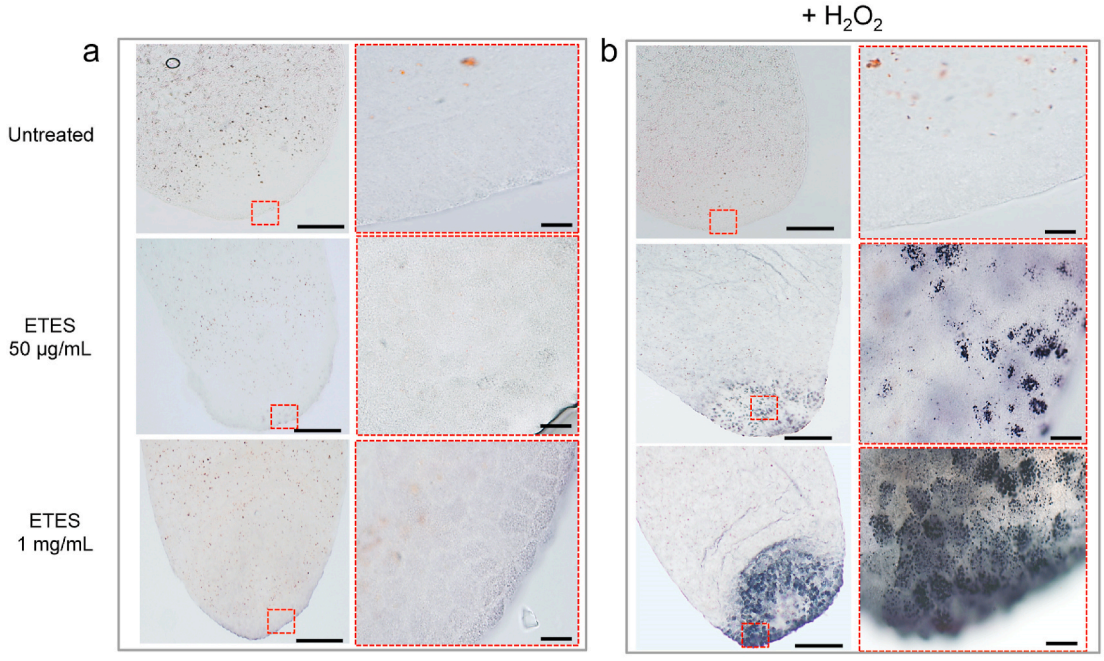

Fig. 3. ETE-S polymerization occurs specifically in basal disc cells.
Fixed polyps were treated at two concentrations with ETE-S in absence a) or presence b) of peroxidase substrate H_2O_2. In each panel, the images on the left column show the peduncle region of untreated and treated animals, while on the right column the regions red framed are shown at higher magnification. In a) a faint staining was detectable at the basal disc level, due to physiological H_2O_2 presence. b) Addition of H_2O_2 (0.17%) induces strong staining of granular structures in basal disc cells, whose amount and intensity increases with ETE-S concentration. Scale bars, 200 μm (a-b, left column) and 20 μm (a-b, right column).

hypothesis that ETE-S could undergo polymerization by mean of endogenous peroxidase, as shown *in vivo* in the plant [9]. ETE-S was added at two concentrations (50 μg/mL and 1 mg/mL) to fixed animals for 30 min, in the absence and presence of H_2O_2. Fig. 3 shows in the first case a faint black staining of the basal disc region, likely resulting from the low physiological amount of hydrogen peroxide inside tissues, which may limit the complete polymerization of ETE-S. These results mirror the *in vivo* staining of Fig. 1. At higher concentration (not compatible with animal life), a strong punctuated pattern was detected in the same cells, further enhanced by exogenous H_2O_2, which thus parallels the peroxidase positive granules well characterized at ultrastructural level by cytochemistry (Fig. S4) [19,21].

Remarkably, under these conditions, a faint dark colour was also detected along the body and in the hypostomal region, at the base of tentacles. These data are also confirmed by spectroscopic analysis that indicate the presence of p(ETE-S) in the body column, and are supported by the expression of different peroxidase-like genes in body ectodermal cells (Fig. S5) [26]. Beside the dose- and H_2O_2- dependent increase of the staining signal, and the cell specificity, indicating a peroxidase-like activity involved in ETE-S polymerization *in vivo,* an additional evidence was also achieved. This was done by inhibiting the peroxidase activity by physical method (high temperature) and by saturating the enzyme with H_2O_2 excess, in diverse solvents (Fig. 4a). The degree of inhibition was estimated by quantifying the staining intensities and grouping into four different categories, ranging from no staining to intense staining (Fig. S6). Pre-heating the animals both at 90 °C and 100 °C could completely prevent the intense staining, allowing some weak staining, index of residual activity. Similar results were obtained by pre-treatment with H_2O_2 in methanol, while less efficient inhibition was found with H_2O_2 in water, or with a lower amount of H_2O_2, where an intense staining could still be detected, although at a lower extent (Fig. S7). Remarkably, the staining observed on the hypostomal region, at the tentacle base, was also prevented (Fig. S5), showing unambiguously the involvement of peroxidase-like activity for *in vivo* and *in vitro* ETE-S polymerization. This activity may be responsible for ETE-S polymerization and for other biotransformations occurring post-secretion, generating a hybrid secreted material with novel functionalities. Indeed, although not demonstrated at functional level, it has been suggested that the peroxidase detected into the granules of basal disc cells could catalyse the crosslinking of other components to post-draw the secreted adhesive, altering the mechanical and physical properties, as it occurs in the freshwater caddisfly silk [29].

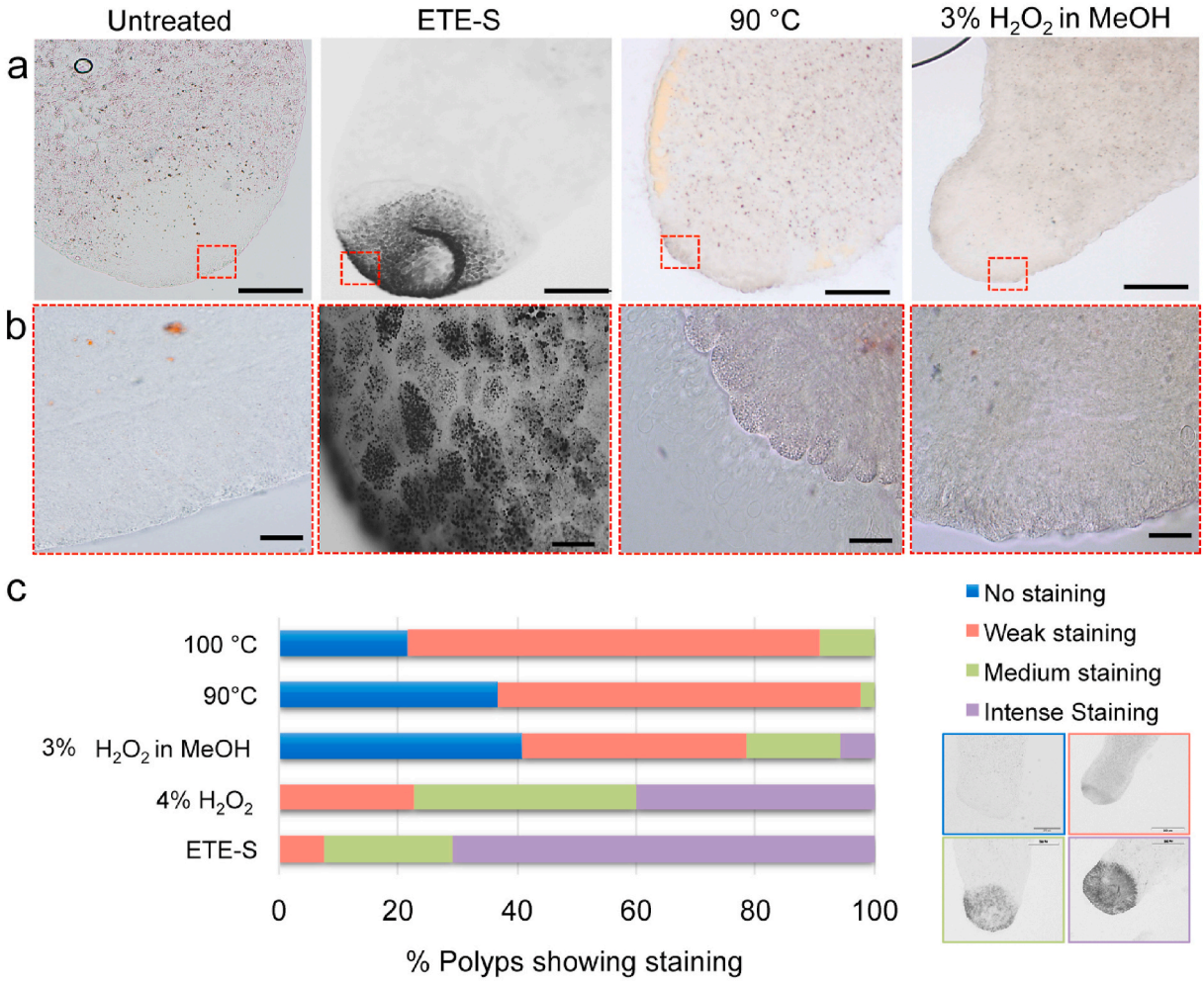

Fig. 4. Inhibition of endogenous peroxidase activity prevents ETE-S polymerization in *Hydra.*
Fixed polyps were chemically and physically pre-treated to inhibit the peroxidase activity, in presence of H_2O_2. a) The regions within the boxes are shown at higher magnification in b). Both high temperature or substrate excess inhibit ETE-S staining. Scale bar 200 μm (a) and 20 μm (b). c) Quantitative evaluation of peroxidase activity inhibition. The Image processing and Analysis software Image J (Version 1.53) was used to quantify and categorize the signal intensity produced by ETE-S polymerization (Fig. S6). Data are reported as the media of three independent experiments (N = 45). Statistical analysis performed using Chi-square test shows highly significant differences (***$p < 0.001$) for each condition compared to the ETE-S treatment.

2.3. Electrical characterization of the ETE-S functionalized structures polymerized in vivo

Next, we proceed to characterize the electrical and electrochemical properties of the secreted discs where the dark polymerized material is arranged as a well-defined ring and which thickness increases with incubation period (Fig. 1, Fig. S2). In order to establish electrical contact with the *Hydra* discs, they were laminated on an Au microelectrode array Fig. 5a–b. To characterize the resistance, we performed IV measurements in the dry state at various interelectrode distances (from 15 to 135 μm) by sweeping the voltage between +0.5 V and −0.5 V while recording the current, see Fig. 5b. For secreted discs produced with 10 μg/mL ETE-S treatment for 24 h, a linear IV was observed, and the current magnitude was decreasing with increasing interelectrode distance following Ohms law (Fig. 5c). The resistance values were in the MΩ range, 3 orders of magnitude lower than the resistance of control untreated secreted discs (Fig. 5d). These values were reproducible for interelectrode distances up to 105 μm suggesting that the polymer granules formed a percolative network over nearly 1/2 of the disc width. Moreover, since we have observed polymerization in the *Hydra* body as well, we attempted to measure the current directly from polyps incubated in ETE-S 50 μg/mL for 24 h, corresponding to the maximum biocompatible dose (Fig. S1). No significant current could be measured, suggesting that p(ETE-S) domains on the body do not form a percolating path in the μm scale as in the discs. In fixed polyps, where the ETE-S dose can be increased to 1 mg/mL, a current higher than control samples could be recorded, but only for an interelectrode distance of 15 μm (Fig. S8).

Next, we characterized the electrochemical properties and electroactivity of p(ETE-S) in an electrolytic environment with a two-electrode electrochemical setup comprising the secreted disc as the working electrode, and an Ag/AgCl pellet as reference/counter electrode. The disc was contacted through the multielectrode array via an open square area that had similar dimensions with the discs while the rest of the array was insulated with a Parylene-C layer in order to eliminate parasitic contribution from the electrodes (Fig. 5b). We first performed cyclic voltammetry with a scan rate of 25 mV/s between −0.5 and +0.5 V vs Ag/AgCl in discs of treated and untreated *Hydra* as well as the electrode area without any biological sample. From the cyclic voltammograms, it is clear that the functionalized secreted disc has a higher capacitance than the untreated sample and the gold electrodes (Fig. 5g; Fig. S9). For this sample we have 10 times higher capacitive currents compared to the gold working electrode, which signifies that the p(ETE-S) domains can store more charge than the gold electrode. While in the gold electrode the capacitance arises from the double layer capacitance at the flat electrode surface, the capacitance in the case of p(ETE-S) is volumetric due to the mixed ionic-electronic transport that p(ETE-S) exhibits. Electrochemical cycling (6 cycles) showed no significant loss of electroactivity (Fig. S10). Additionally, we performed charge-discharge curves at different applied currents in order to extract the capacitance of the sample (Fig. 5h). We observed that the curves deviate from the ideal linear behaviour of a supercapacitor, something that can be attributed to non-ideal contacts that can generate Faradaic redox reactions. From the slope of the linear part of the discharge curve we extracted the capacitance of our system to equal C = 1 μF. Assuming that the p(ETE-S) specific capacitance is 20 F/cm^3 as it was determined in the plant tissue [8] the conducting material in the disc corresponds to a volume of 5 10^4 μm^3. We always observed increased capacitance and electroactivity in the ETE-S functionalized secreted discs, but the current magnitude was different between samples. Although the same experimental conditions were used during *Hydra* incubation in ETE-S, the diverse degree of polymerization and polymer formation on the basal discs reflects animal variability.

Overall, the electrical and electrochemical characterizations show that the conjugated oligomer polymerized *in vivo* forms polymer domains with percolation paths supporting electronic conduction. The tissue-integrated conjugated polymer can be further doped and dedoped electrochemically via exchange of ions with an electrolyte. *In vivo*

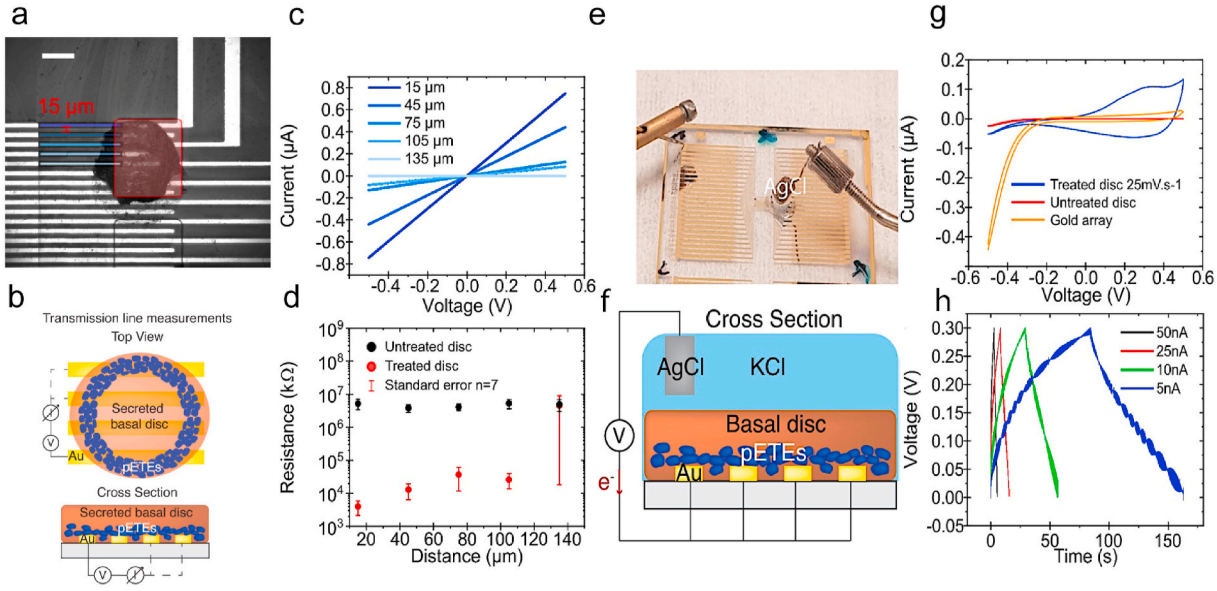

Fig. 5. Electrical and electrochemical characterization of the ETE-S functionalized secreted discs via a planar gold multielectrode array.
a) Image of a secreted disc on top of the delimited non insulated area (red square) of the Au multielectrode array with contacts from 15 μm to 135 μm represented with blue lines from dark to light. Scale bar, 50 μm. b) Schematic of the transmission line measurement setup. Secreted discs are dried on top of the patterned gold electrodes. The current is then measured at different interelectrode distances. The blue grains represent the granular structure of the p(ETE-S) domains in the *Hydra* secreted disc. c) IV curves for interelectrode distances from 15 to 135 μm (dark to light blue) and d) corresponding resistance values of secreted discs from treated (blue) and untreated *Hydra* (red); Standard error from n = 7. e) Photograph and f) schematic of the 2–electrodes electrochemical setup with an Ag/AgCl pellet as Reference/Counter electrode and the disc as the working electrode in a 0.1 M KCl electrolyte. g) Cyclic voltammogram at 25 mV/s vs Ag/AgCl from the non-insulated gold electrodes area (yellow), the secreted disc from untreated (red) and *Hydra* treated with 10 μg/mL ETE-S (blue). h) Charge/discharge curves between 0 V and +0.3 V from a treated *Hydra's* secreted disc for applied currents of 50 nA (black), 25 nA (red), 10 nA (green) and 5 nA (blue).

polymerization of a conjugated oligomer has previously only been observed in plants promoted via the cell wall machinery of the plant cells. *Hydra* is the first animal that shows this possibility via the peroxidase enzyme activity contained in the secretory granules. The capability of *Hydra* to use ETE-S as substrate for intracellular polymerization and cross-linking reactions with adhesive mucous material pave the way for utilizing *Hydra* for *in vivo* biofabrication of hybrid functional materials.

2.4. ETE-S staining as marker of basal disc cell differentiation

The finding that ETE-S polymerization is mediated by endogenous peroxidase led us to use ETE-S as biochemical marker for tracking the reappearance of basal disc cells during polyps budding and regeneration. *Hydra* in laboratory conditions reproduce asexually via budding, which starts with tissue outgrowth at the gastric region level, gradually shaping head and tentacles and growing up to detachment of the new individual (Fig. 6a). The cells closer to the mother body gradually differentiate into basal disc cells, progressively acquiring peroxidase activity [28]. Basal disc cells differentiation occurs also during foot regeneration (Fig. 6d), starting from 12 h post amputation (p.a.) and reaching highest level after 48 h (Fig. S4) [28,30]. Both processes can be monitored using chromogenic substrates, such as DAB or ABTS on fixed specimens [28], as the toxicity of the chromogen prevents *in vivo* assays. ETE-S was thus employed as a chromogenic substrate to detect endogenous peroxidase on fixed samples. ETE-S signal was detectable in the late stage of bud development (Fig. 6b–c), and 48 h p.a. (Fig. 6e), according to the dynamic of basal disc cells differentiation of both processes. Due to absence of toxicity at low doses, but still effective in promoting polymerization, we also exploited the possibility to use ETE-S to detect endogenous peroxidase *in vivo*. Amputated bodies were allowed to regenerate their foot in presence of biocompatible dose of ETE-S (10 μg/mL) and H_2O_2 (0.003%). Fig. 6f shows the expected dynamic of mucous production in regenerating polyps, accompanied by progressive darkening, indicating ETE-S polymerization and secretion by neo-differentiated basal disc cells. The enhancing action of H_2O_2 on *in vivo* ETE-S polymerization was confirmed also in adult polyps in homeostatic condition, as shown by the faster production of the black secreted disc in presence of H_2O_2 (Fig. S11). The possibility to perform *in vivo* peroxidase-catalyzed cytochemistry by means of a non-toxic substrate, producing a highly stable and specific staining, represents an innovative powerful tool for morpho-functional studies in dynamic condition.

3. Conclusions

In conclusion we demonstrated a self-organized bioelectronic interface in the invertebrate model organism *Hydra vulgaris* via *in vivo* polymerization of a conjugated oligomer. ETE-S polymerized in the *Hydra* forming conducting and capacitive regions that were seamlessly integrated within the tissue and in the secreted mucous material. We showed that the polymerization was driven by peroxidase activity, as previously observed in plants. We hypothesize that ETE-S is integrated into the *Hydra* tissue during the production of the glue-components in the basal disc region resulting into a novel self-structured biological matrix with electrical properties and therefore extending the possibilities for biofabrication of hybrid materials. Furthermore, the low toxicity of ETE-S enabled us to follow the dynamics of peroxidase expressing cells *in vivo*, initiating new strategies for *in vivo* peroxidase cytochemistry for morpho-functional studies. With our approach we pave the way for self-organized electronics in animal tissue that can be a handle for manipulating biological functions in physiological processes or pathological contexts. Finally, *Hydra* being a model organism for studies of the neural system [31,32], seamlessly integrated electrodes can be used for investigating the effect of conducting materials in the neurons' firing and plasticity.

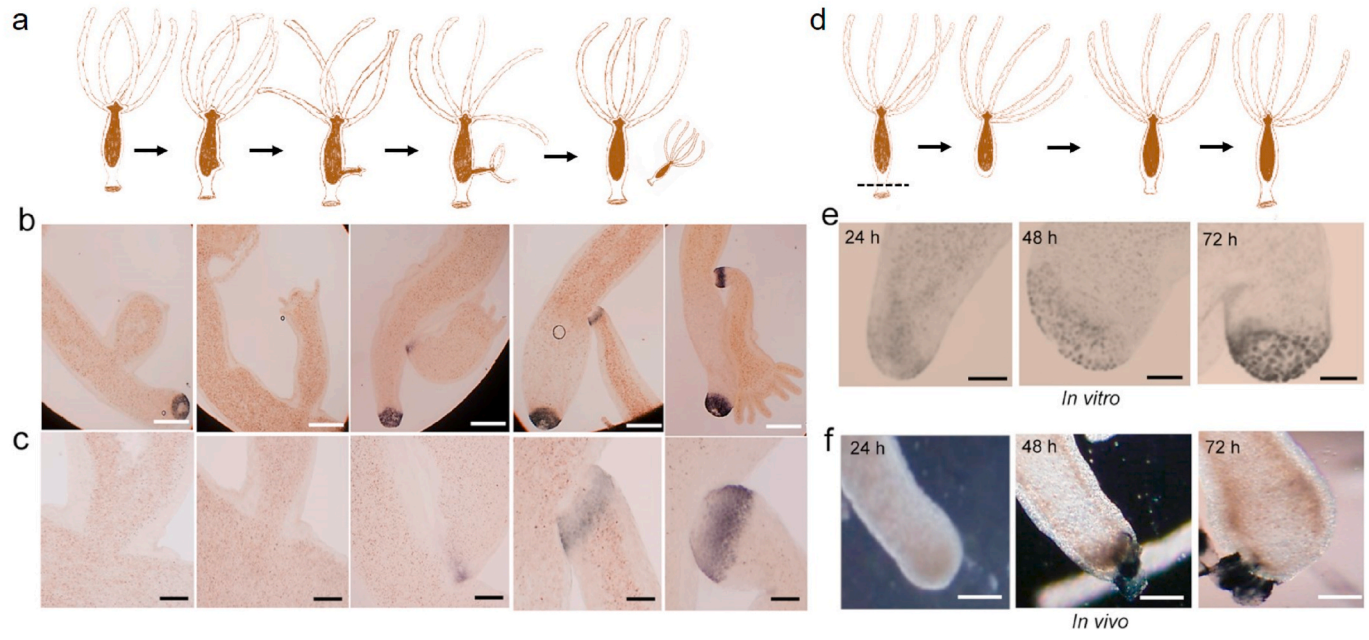

Fig. 6. ETE-S polymerization is a marker of basal disc cell differentiation.
a) Schematic representation of the budding process in Hydra. b) Polyps at different budding stages (developing from left to right) were fixed and then treated with ETE-S in presence of H_2O_2. ETE-S staining is detectable in differentiating basal disc cells, located at base of the budding polyp. c) Higher magnifications of the bud detachment regions in adult and budding *Hydra*. Scale bar, 500 μm (b) and 100 μm (c). d) Schematic representation of foot regeneration when amputation is done at 20% of the body length. e) 24 h, 48 h and 72 h p.a. polyps were fixed and treated with ETE-S in presence of H_2O_2. Localization of dark granules mirrors the distribution of basal disc cells. Scale bars 100 μm. f) *In vivo* detection of basal disc cell activity in regenerating foot. Following body amputation as above, regenerating animals were continuously incubated with ETE-S 10 μg/mL and H_2O_2 (0.003%). Black secreted material is evident from 48 h onwards. Scale bar 100 μm.

4. Methods

4.1. Synthesis of ETE-S trimer

A detailed description of the synthesis and characterization of the ETE-S trimer was recently published elsewhere [33].

4.2. Animal culture

Hydra vulgaris were asexually cultured in Hydra medium (1 mM $CaCl_2$ and 0.1 mM $NaHCO_3$, pH 7), according to the method of Loomis and Lenhoof [34]. Polyps were fed three time per week with freshly hatched *Artemia salina* nauplii and kept at 18 ± 1 °C with a 12:12 h light: dark regime. For all the experiments, polyps starved for 24 h were selected from a homogeneous population.

4.3. In vivo ETE-S polymerization

In a typical experiment, groups of 50 polyps were treated with 300 μL of ETE-S 10 μg/mL for desired time, in a plastic multiwell, then extensively washed and used for further processing. Untreated polyps soaked in Hydra medium were used as controls.

4.4. In vitro ETE-S staining on fixed hydra

Adult polyps with no buds were selected from a homogeneous population and fixed according to the following protocol: 5 min relaxation in urethane 2% in Hydra medium, fixation in paraformaldehyde (PFA) 4% for 2 h at 18 °C, and extensive washing in Hydra medium. ETE-S from stock solution (4 mg/mL) was diluted in Hydra medium to obtain working solutions of 1 mg/mL and 50 μg/mL. Fixed polyps were soaked for 30 min in ETE-S at 50 μg/mL or 1 mg/mL, then extensively washed with Hydra medium and mounted on microscopy slides. For the staining in presence of H_2O_2, a 10 min co-incubation with freshly prepared 0.17% H_2O_2 (50 mM) was performed. The control experiment was carried out by treating fixed polyps with 0.17% H_2O_2 for 10 min. Microscopy analysis was performed by using an inverted microscope (Axiovert 100, Zeiss, Jena, Germany) equipped with a digital colour camera (Olympus, DP70). The software Cell F (Olympus) was used for imaging acquisition and analysis.

In order to track down the gradual restoration of foot peroxidase activity during its regeneration, a staining procedure was carried out on adult budless animals using the chromogen 3,3′-Diaminobenzidine (DAB) at different timepoints post-amputation. After a bisection at 20% of the body length, amputated polyps were relaxed in urethane 2% in Hydra medium for 2 min and then fixed in PFA 4% in Hydra medium for 2 h at 18 °C. Fixation of regenerating animals was carried out at 16, 24, 36 or 48 h after the bisection occurred. Following washes of fixed animals with PBS to remove any residual fixative, polyps were incubated for 15 min with 2 mL of DAB solution, prepared beforehand according to the manufacturer's instructions (Sigma-Aldrich tablets). The colorimetric reaction was stopped by washing the animals five times with Di water. Polyps were then mounted with PBS/Glycerol 1:1 on microscope slides for image acquisition, using the same microscope and camera used for the microscopy analysis performed on ETE-S stained animals.

4.5. In vitro peroxidase inhibition

We carried out two different strategies in order to inhibit the peroxidase activity: enzyme saturation pre-treating the samples with high dose of H_2O_2 and enzyme denaturation using high temperature. For inhibition by enzyme saturation groups of 15 budless polyps were fixed with PFA 4%, then soaked for 90 min with freshly prepared 4% H_2O_2 in water and 3% H_2O_2 in Methanol. For inhibition by heating, polyps were boiled either 10 min at 90 °C or 2 min at 100 °C. After these pretreatments the samples were washed three times in Hydra medium for 5 min, then stained with H_2O_2/ETE-S solution (0.17% H_2O_2 in 1 mg/mL ETE-S) for 10 min. The samples were washed three times in Hydra medium and mounted on microscopy slides. As control condition, ETE-S staining with H_2O_2 was performed on non-pretreated polyps. Quantification of peroxidase inhibition was accomplished as it follows: fixed animals were imaged by an inverted microscope (Axiovert 100, Ziess) under the same conditions of acquisition (light and exposure time), saved in tagged-image file format (TIFF) at a size of 1360 × 1024 pixels for data processing using the Image processing and Analysis software Image J (Version 1.53). Colorimetric intensities expressed as a.u. were grouped into four classes (zero, low, medium and high, defined in Fig. S6). The data are expressed as percentage of polyps belonging to each category, and the experiment was repeated three times for each tested condition.

4.6. In vitro ETE-S staining during budding development and foot regeneration

To track the reappearance of basal disc cells in physiological processes using ETE-S, budding polyps at several stage of development were chosen from a homogeneous population and fixed with PFA 4% (see method above). The fixed samples were soaked for 10 min with H_2O_2/ETE-S solution (0.17% H_2O_2 in 1 mg/mL ETE-S) and then washed three times with *Hydra* medium. The samples were arranged on slides for microscopy analysis. ETE-S staining during the foot regeneration: groups of 15 budless polyps were selected and the foot amputation performed with a scalpel at 20% of the body length. The footless polyps were collected in a plastic multiwell and cultured in 1 mL of Hydra medium at 18 °C. After 24 h and 48 h from the cutting, the regenerants were fixed in PFA 4% and the ETES staining with H_2O_2 was carried out (see method above). The experiment was repeated three times for each tested condition.

4.7. Uv–Vis spectroscopy

The Uv–vis spectroscopy was performed on crude homogenates prepared from whole animals (220 polyps) treated 24 h with ETE-S 50 μg/mL, or after sectioning to separate body columns from foot regions. All collected specimens were mechanically crushed with a pestle in DMSO (5 μL per polyp), then allowed to stand to promote the debris precipitation and supernatants collection. As a control, the same homogenates were obtained from untreated polyps. UV–Vis spectra were obtained using a microplate reader Biotek, Synergy H1 between 350 and 800 nm with a resolution of 1 nm. Obtained data were normalized to the minimum value before removing the DMSO blank from the sample data. The resultant curves were smoothed using the adjacent-average method for a window of N = 50 pts.

4.8. Spectromicroscopy

Treated polyps (ETE-S 50 μg/mL) and corresponding detached secreted discs were dried on microscope slides. Fixed polyps were mounted in PBS/glycerol 50%. The stained polyps were then mounted in a PBS/Glycerol 50% solution. Absorbance microscopy was obtained using a Nikon Eclipse L200 N optical microscope (halogen lamp 50 *W*) with an objective lens of 50× magnification (NA = 0.8). Transmitted light was collected from the camera with a guiding light (optical fibre 105 μm) connected to a spectrophotometer (OceanOptics, HR 4000, USA) and absorption spectra (400–900 nm) of selected regions were then acquired. Collected spectra were averaged from 5 successive spectra obtained with an integration time of 100 ms. Respective reference for dried and mounted polyps were the glass slide and the mounted glass slide.

4.9. Multielectrode array fabrication

The fabrication started by cleaning glass slides of 1 × 3 inches. First the glass slides were immersed in Di water with 2% Decon-90 detergent and sonicated for 15 min. Then after thorough rinsing, the glass slides were immersed in 80% acetone with 20% Isopropanol mixture and sonicated for 20 min. Finally, the samples were dried with N_2 and an O_2 plasma activation step with parameters: O_2: 500 sccm, RF 100, pressure 500 mTorr, for 120 s. After the plasma treatment, 5 nm of Cr and 100 nm of Au were evaporated. Then, s1805 was spin coated on top of Au at 3000 rpm for 30 s and baked for 60 s at 110 C under vacuum for 1 min. The samples were exposed in UV g line (10 mj/cm^2) for 2 s in a Karl Suss MA6 mask aligner. The samples were developed with MF26A developer for 30 s, rinsed with di water and dried with N_2. Au was etched by an Au etchant, and Cr was etched by an Cr etchant purchased at Aldrich. To remove the remaining photoresist, the samples were soaked in Acetone, dried with N_2, activated with O_2 plasma as before. Parylene-C with thickness of 2 μm was deposited, with 3-(methoxysilyl)propyl methacrylate (silane A-174) by using a Diener parylene coater. Silane A174, was used as an adhesion promoter between Parylene and glass substrate. Finally, a second photolithography step was performed to expose the active Au area and insulate the rest of lines. For that step, AZ-10XT was spin-coated at 3000 rpm for 30 s, baked at 110 C for 2 min, exposed for 14 s, and developed for 2 min with an AZ developer. Finally, a plasma etching step (O_2 500 sccm, CF4 100 sccm, RF 160, Pressure 200 mTorr, for 5min) etched the parylene at the active areas, while the rest was protected by the photoresist. The samples were immersed in acetone to remove the remaining photoresist, and dried with N_2.

4.10. Electrical characterization of hydra secreted discs

Electrical and electrochemical measurements were performed with a Keithley 2612B Source-Measure Unit. The secreted basal disc was contacted through an Au multielectrode array via an open square area that had dimensions matching with the discs while the rest of the array was insulated with a Parylene-C layer in order to eliminate parasitic contribution from the electrodes. The microelectrode array was contacted using a micromanipulator from Quarter Research (model XYZ TR 300) with tips from Signatone (SE-T). IV were obtained with a scan rate of 25 mV/s between −0.5 and +0.5 V. Resistance was obtained by measuring the slope of the linearly fitted IV-curves for each interelectrode distance. Cyclic voltammetry was performed in a 2-electrodes electrochemical set-up with an Ag/AgCl pellet as a Reference/Counter electrode and the secreted disc as the working electrode. The electrolyte was 0.1 M KCl and the scan rate 25 mV/s. The contacts of the gold lines defining the working electrode area were shorten using a silver paste. Galvanostatic charge/discharge curves were obtained from 0V to 0.3 V vs Ag/AgCl for applied current ranging from 5 to 50 nA. Capacitance was calculated from the slope of the discharge curve using the following equation:

$$C = I \Big/ \left(\frac{dV}{dt}\right)$$

where I is the applied current and dV/dt, the slope of the linear part of the discharge curve.

Credit author statement

Giuseppina Tommasini, Gwennaël Dufil: Methodology, Validation, Formal analysis, Investigation, writing/orginal draft; Federica Fardella, Xenofon Strakosas: Methodology, Investigation, Visualization. Eugenio Fergola: Investigation; Tobias Abrahamsson, David Bliman, Roger Olsson: investigation, Resources; Magnus Berggren, Angela Tino: Data curation, Supervision; Claudia Tortiglione, Eleni Stavrinidou: Conceptualization, Supervision, Methodology, Writing – review & editing.

Declaration of competing interest

Authors declare that they have no competing interests.

Acknowledgments

The authors wish to thank Roger Gabrielsson (Linköping University) for synthesis of ETE-S at the early stages of the study. This work was supported by the European Union's Horizon 2020 research and innovation programme under grant agreement No 800926 (FET-OPEN-HyPhOE) and by the Swedish Research Council (VR-2017-04910). Additional funding was provided by the Knut and Alice Wallenberg Foundation, the Swedish Foundation for Strategic Research (SSF), The European Research Council (ERC) project e-NeuroPharma 834677 and the Swedish Government Strategic Research Area in Materials Science on Advanced Functional Materials at Linköping University (Faculty Grant SFO-Mat-LiU No. 2009-00971). DB and R. are supported by MultiPark - A Strategic Research Area at Lund University. GT thanks the MIUR project SHARID - ARS01-01270 for financial support. Fig. 1f and 2c were created with Biorender.com.

Appendix A. Supplementary data

Supplementary data to this article can be found online at https://doi.org/10.1016/j.bioactmat.2021.08.025.

References

[1] A.F. Renz, J. Lee, K. Tybrandt, M. Brzezinski, D.A. Lorenzo, M. Cerra Cheraka, J. Lee, F. Helmchen, J. Vörös, C.M. Lewis, Opto-E-dura: a soft, stretchable ECoG array for multimodal, multiscale neuroscience, Advanced Healthcare Materials 9 (17) (2020) 2000814.

[2] G. Schiavone, F. Fallegger, X. Kang, B. Barra, N. Vachicouras, E. Roussinova, I. Furfaro, S. Jiguet, I. Seáñez, S. Borgognon, A. Rowald, Q. Li, C. Qin, E. Bézard, J. Bloch, G. Courtine, M. Capogrosso, S.P. Lacour, Soft, implantable bioelectronic interfaces for translational research, Adv. Mater. 32 (17) (2020) 1906512.

[3] D. Khodagholy, J.N. Gelinas, T. Thesen, W. Doyle, O. Devinsky, G.G. Malliaras, G. Buzsáki, NeuroGrid: recording action potentials from the surface of the brain, Nat. Neurosci. 18 (2) (2015) 310–315.

[4] L. Xu, S.R. Gutbrod, Y. Ma, A. Petrossians, Y. Liu, R.C. Webb, J.A. Fan, Z. Yang, R. Xu, J.J. Whalen 3rd, J.D. Weiland, Y. Huang, I.R. Efimov, J.A. Rogers, Materials and fractal designs for 3D multifunctional integumentary membranes with capabilities in cardiac electrotherapy, Adv. Mater. 27 (10) (2015) 1731–1737.

[5] T. Zhou, G. Hong, T.-M. Fu, X. Yang, T.G. Schuhmann, R.D. Viveros, C.M. Lieber, Syringe-injectable mesh electronics integrate seamlessly with minimal chronic immune response in the brain, in: Proceedings of the National Academy of Sciences, 2017, p. 201705509.

[6] J. H, S.M. Richardson-Burns, D.C. Martin, Electrochemical polymerization of conducting polymers in living neural tissue, J. Neural. Eng. 4 (2) (2007) L6–L13.

[7] J. Liu, Y.S. Kim, C.E. Richardson, A. Tom, C. Ramakrishnan, F. Birey, T. Katsumata, S. Chen, C. Wang, X. Wang, L.-M. Joubert, Y. Jiang, H. Wang, L.E. Fenno, J.B. H. Tok, S.P. Paşca, K. Shen, Z. Bao, K. Deisseroth, Genetically targeted chemical assembly of functional materials in living cells, tissues, and animals, Science 367 (6484) (2020) 1372.

[8] E. Stavrinidou, R. Gabrielsson, K.P. Nilsson, S.K. Singh, J.F. Franco-Gonzalez, A. V. Volkov, M.P. Jonsson, A. Grimoldi, M. Elgland, I.V. Zozoulenko, D.T. Simon, M. Berggren, *In vivo* polymerization and manufacturing of wires and supercapacitors in plants, Proc. Natl. Acad. Sci. U. S. A. 114 (11) (2017) 2807–2812.

[9] G. Dufil, Daniela Parker, Jennifer Y. Gerasimov, Thuc-Quyen Nguyen, Magnus Berggren, Eleni Stavrinidou, Enzyme-assisted *in vivo* polymerisation of conjugated oligomer-based conductors, J. Mater. Chem. B 8 (2020) 4221–4227.

[10] D. Mantione, E. Istif, G. Dufil, L. Vallan, D. Parker, C. Brochon, E. Cloutet, G. Hadziioannou, M. Berggren, E. Stavrinidou, E. Pavlopoulou, Thiophene-based trimers for *in vivo* electronic functionalization of tissues, ACS Applied Electronic Materials 2 (12) (2020) 4065–4071.

[11] M. Allocca, L. Mattera, A. Bauduin, B. Miedziak, M. Moros, L. De Trizio, A. Tino, P. Reiss, A. Ambrosone, C. Tortiglione, An integrated multilevel analysis profiling biosafety and toxicity induced by indium- and cadmium-based quantum dots *in vivo*, Environ. Sci. Technol. 53 (7) (2019) 3938–3947.

[12] A. Ambrosone, M. Roopin, B. Pelaz, A.M. Abdelmonem, L.M. Ackermann, L. Mattera, M. Allocca, A. Tino, M. Klapper, W.J. Parak, O. Levy, C. Tortiglione, Dissecting common and divergent molecular pathways elicited by CdSe/ZnS quantum dots in freshwater and marine sentinel invertebrates, Nanotoxicology 11 (2) (2017) 289–303.

[13] C. Tortiglione, A. Quarta, M.A. Malvindi, A. Tino, T. Pellegrino, Fluorescent nanocrystals reveal regulated portals of entry into and between the cells of Hydra, PloS One 4 (11) (2009), e7698.
[14] V. Marchesano, Y. Hernandez, W. Salvenmoser, A. Ambrosone, A. Tino, B. Hobmayer, J. M de la Fuente, C. Tortiglione, Imaging inward and outward trafficking of gold nanoparticles in whole animals, ACS Nano 7 (3) (2013) 2431–2442.
[15] G. Veronesi, M. Moros, H. Castillo-Michel, L. Mattera, G. Onorato, K.D. Wegner, W. L. Ling, P. Reiss, C. Tortiglione, *In vivo* biotransformations of indium phosphide quantum dots revealed by X-ray microspectroscopy, ACS Appl. Mater. Interfaces 11 (39) (2019) 35630–35640.
[16] M. Moros, F. Di Maria, P. Dardano, G. Tommasini, H. Castillo-Michel, A. Kovtun, M. Zangoli, M. Blasio, L. De Stefano, A. Tino, G. Barbarella, C. Tortiglione, *In vivo* bioengineering of fluorescent conductive protein-dye microfibers, iScience 23 (4) (2020) 101022.
[17] C. Tortiglione, M.R. Antognazza, A. Tino, C. Bossio, V. Marchesano, A. Bauduin, M. Zangoli, S.V. Morata, G. Lanzani, Semiconducting polymers are light nanotransducers in eyeless animals, Science advances 3 (1) (2017), e1601699.
[18] M. J, B. Hobmayer, D. Eder, M.-K. Eder, S. Glasauer, S. Gufler, M. Hartl, W. Salvenmoser, Stemness in Hydra - a current perspective, Int. J. Dev. Biol. 56 (2012) 509–517.
[19] M. Rodrigues, P. Leclère, P. Flammang, M.W. Hess, W. Salvenmoser, B. Hobmayer, P. Ladurner, The cellular basis of bioadhesion of the freshwater polyp Hydra, BMC Zoology 1 (1) (2016) 3.
[20] L. Davis, Histological and ultrastructural studies of the basal disk of Hydra, Z. Zellforsch. Mikrosk. Anat. 139 (1973) 1–27.
[21] D. H, S.A.H. Hoffmeister-Ullerich, J. Kielholz, M. Schweizer, H.C. Schaller, Isolation of a putative peroxidase, a target for factors controlling foot-formation in the coelenterate Hydra, Eur. J. Biochem. 269 (2002) 4597–4606.
[22] F. G, B. Quinn, C. Blaise, Hydra, a model system for environmental studies, Int. J. Dev. Biol. 56 (6) (2012) 613–625.
[23] O.K. Wilby, J.M. Tesh, The Hydra assay as an early screen for teratogenic potential, Toxicol. Vitro : an international journal published in association with BIBRA 4 (4–5) (1990) 582–583.
[24] E. Stavrinidou, R. Gabrielsson, E. Gomez, X. Crispin, O. Nilsson, D.T. Simon, M. Berggren, Electronic plants, Science advances 1 (10) (2015), e1501136.
[25] A.V. Volkov, S.K. Singh, E. Stavrinidou, R. Gabrielsson, J.F. Franco-Gonzalez, A. Cruce, W.M. Chen, D.T. Simon, M. Berggren, I.V. Zozoulenko, Spectroelectrochemistry and nature of charge carriers in self-doped conducting polymer, Advanced Electronic Materials 3 (8) (2017) 1700096.
[26] T. O, M. Rodrigues, L. Kremeser, H. Lindner, C. Beisel, E. Berezikov, B. Hobmayer, P. Ladurner, Profiling of adhesive-related genes in the freshwater cnidarian Hydra magnipapillata by transcriptomics and proteomics, Biofouling 32 (9) (2016) 1115–1129, 2016 Oct;32(9.
[27] T. B, S. Thomsen, Foot differentiation and genomic plasticity in Hydra: lessons from the PPOD gene family, Dev. Gene. Evol. 216 (2) (2006) 57–68.
[28] H. S, S. Hoffmeister, A new biochemical marker for foot-specific cell differentiation in Hydra, Wilhelm Rouxs Arch Dev Biol 194 (1985) 453–461.
[29] C.-S. Wang, N.N. Ashton, R.B. Weiss, R.J. Stewart, Peroxinectin catalyzed dityrosine crosslinking in the adhesive underwater silk of a casemaker caddisfly larvae, Hysperophylax occidentalis, Insect Biochem. Mol. Biol. 54 (2014) 69–79.
[30] S. Gufler, B. Artes, H. Bielen, I. Krainer, M.K. Eder, J. Falschlunger, A. Bollmann, T. Ostermann, T. Valovka, M. Hartl, K. Bister, U. Technau, B. Hobmayer, β-Catenin acts in a position-independent regeneration response in the simple eumetazoan Hydra, Dev. Biol. 433 (2) (2018) 310–323.
[31] C. Dupre, R. Yuste, Non-overlapping neural networks in Hydra vulgaris, Curr. Biol. 27 (8) (2017) 1085–1097.
[32] P. Pierobon, C. Sogliano, R. Minei, A. Tino, P. Porcu, G. Marino, C. Tortiglione, A. Concas, Putative NMDA receptors in Hydra: a biochemical and functional study, Eur. J. Neurosci. 20 (10) (2004) 2598–2604.
[33] J.Y. Gerasimov, D. Zhao, A. Sultana, T. Abrahamsson, S. Han, D. Bliman, D. Tu, D. T. Simon, R. Olsson, X. Crispin, M. Berggren, S. Fabiano, A biomimetic evolvable organic electrochemical transistor, Advanced Electronic Materials n/a (2021) 2001126, n/a.
[34] W.F. Loomis, H.M. Lenhoff, Growth and sexual differentiation of Hydra in mass culture, J. Exp. Zool. 132 (1956) 555–574.